JGR Oceans

RESEARCH ARTICLE
10.1029/2020JC016095

Wintertime Coastal Upwelling in Lake Geneva: An Efficient Transport Process for Deepwater Renewal in a Large, Deep Lake

Rafael S. Reiss[1], U. Lemmin[1], A. A. Cimatoribus[1], and D. A. Barry[1]

[1]Ecological Engineering Laboratory (ECOL), Faculty of Architecture, Civil and Environmental Engineering (ENAC), Ecole Polytechnique Fédérale de Lausanne (EPFL), Lausanne, Switzerland

Abstract Combining field measurements, 3-D numerical modeling, and Lagrangian particle tracking, we investigated wind-driven, Ekman-type coastal upwelling during the weakly stratified winter period 2017/2018 in Lake Geneva, Western Europe's largest lake (max. depth 309 m). Strong alongshore wind stress, persistent for more than 7 days, led to tilting and surfacing of the thermocline (initial depth 75–100 m). Observed nearshore temperatures dropped by 1°C and remained low for 10 days, with the lowest temperatures corresponding to those of hypolimnetic waters originating from 200 m depth. Nearshore current measurements at 30 m depth revealed dominant alongshore currents in the entire water column (maximum current speed 25 cm s^{-1}) with episodic upslope transport of cold hypolimnetic waters in the lowest 10 m mainly during the first 3 days. The observed upwelling dynamics were well reproduced by a 3-D hydrodynamic model (RMSE 0.2°C), whose results indicated that upwelled waters spread over approximately 10% of the lake's main basin surface area. Model-based Lagrangian particle tracking confirmed that upwelled waters originated from far below the thermocline, that is, >150 m depth, and descended back to around 150–200 m depth over a wide area after wind stress ceased. Observational and particle tracking results suggest that wintertime coastal upwelling, which can occur several times during winter, is an overlooked transport process that is less sensitive to the effects of global warming than convective cooling. It can provide an effective but complex 3-D pathway for deepwater renewal in Lake Geneva, and other large, deep lakes with a sufficiently long wind fetch.

Plain Language Summary Freshwater lakes are increasingly important as drinking water sources and for societal and economic activities. To maintain good water quality, deepwater renewal is essential for lake ecosystems. Traditionally, convectively driven vertical mixing during wintertime is considered as one of the main processes for deepwater renewal. In deep lakes, this mixing often cannot reach down to the deepest layers. Since this situation is expected to worsen due to climate change-induced warming, a good understanding of alternative deepwater renewal processes is crucial. We investigate wind-driven coastal upwelling of hypolimnetic water during the weakly stratified winter period. The study was carried out in monomictic Lake Geneva, a large, deep lake (depth 309 m), combining field observations, 3-D hydrodynamic modeling, and Lagrangian particle tracking, an effective combination for addressing the complex 3-D upwelling dynamics over a large area of the lake. We show that coastal upwelling can lift water masses from far below the thermocline up to the surface in the nearshore region, where they spend up to 5 days before descending back to the deeper layers. Our results demonstrate that wintertime coastal upwelling, an as yet overlooked transport process, can efficiently contribute to the renewal and aeration of the deepwater layer in deep lakes.

Key Points:
- Coastal upwelling during winter in a large deep lake was investigated by field observations, 3-D numerical modeling, and particle tracking
- Upwelled water masses originating from the deep hypolimnion spend up to 5 days near the surface before descending back into that layer
- Wintertime coastal upwelling is an efficient yet overlooked process for deepwater renewal in large deep lakes with favorable wind conditions

Supporting Information:
- Supporting Information S1
- Movie S1

Correspondence to:
R. S. Reiss,
rafael.reiss@epfl.ch

Citation:
Reiss, R. S., Lemmin, U., Cimatoribus, A. A., & Barry, D. A. (2020). Wintertime coastal upwelling in Lake Geneva: An efficient transport process for deepwater renewal in a large, deep lake. *Journal of Geophysical Research: Oceans*, *125*, e2020JC016095. https://doi.org/10.1029/2020JC016095

Received 17 JAN 2020
Accepted 19 JUL 2020
Accepted article online 3 AUG 2020

1. Introduction

Convective winter cooling is an important process in the annual cycle of many lake ecosystems. It transports oxygen-rich waters from the surface to the deeper parts and recycles nutrients. However, in deep monomictic lakes, convectively induced vertical transport and mixing are often not sufficient to reach the lake's deepest layers (Coats et al., 2006; Livingstone, 1993; Perroud et al., 2009). Driven by the temperature differences between the atmosphere and the lake surface, convective cooling is expected to become even less efficient in the future with potentially milder winters due to climate change (Adrian et al., 2009; Ambrosetti & Barbanti, 1999; Goldman et al., 2013; O'Reilly et al., 2015; Sahoo et al., 2013; Wahl & Peeters, 2014). Such

a reduction of convectively induced deepwater renewal might result in lower dissolved oxygen (DO) concentrations, causing potentially negative effects for the lake's ecological health (e.g., Friedrich et al., 2014; Likens, 2010).

In large, deep lakes, two other processes originating in the coastal zone can significantly contribute to deepwater renewal during wintertime: density currents on the lateral slopes caused by differential cooling between the shallow literal zone and the deep offshore region (Fer et al., 2002; Peeters et al., 2003) and upwelling of deepwater masses over the lateral slopes, which results from wind forcing and may be affected by Coriolis forcing (e.g., Csanady, 1977; Schladow et al., 2004). The former is a special case of convective cooling and as such may decrease in importance because of climate change. The latter, on the other hand, is wind-driven and thus less sensitive to increasing air temperatures.

Observations and qualitative descriptions of coastal upwelling in the ocean date back more than a century (e.g., McEwen, 1912; Schulz, 1917; Thorade, 1909). The phenomenon could be explained by Ekman's then recent work on the influence of the Earth's rotation on ocean currents (Ekman, 1905), whereby persistent wind stress results in surface layer transport that is perpendicular to the direction of the wind (to the right in the Northern Hemisphere). In the nearshore region, this divergence in the surface layers must be compensated for by upwelling of colder waters from below or by downwelling of near-surface water masses, depending on the direction of the wind. Upwelling events are classified as "partial" (the thermocline does not reach the surface) or "full" (the thermocline surfaces) (Csanady, 1977).

Depending on the basin size and fetch length, coastal upwelling in lakes takes on different forms. In small (in terms of Rossby radius) lakes, direct upwelling occurs at the upwind end (Coman & Wells, 2012; Mortimer, 1952). Pöschke et al. (2015) used airborne thermal imagery and in situ temperature observations to investigate upwelling in two small temperate lakes. They concluded that wind-driven upwelling could be at least as important as convective cooling for deep mixing and hypolimnetic oxygen renewal during the spring overturn in such systems. The same type of upwelling takes place in larger lakes in which Coriolis force-induced Poincaré and/or Kelvin waves are observed, but which have limited fetch, such as Lake Simcoe (Cossu & Wells, 2013), Lake Tahoe (Steissberg et al., 2005), and Lake Biwa (Homma et al., 2016). Similar to the ocean, Ekman-type upwelling occurs in large, deep lakes with sufficiently long fetch (e.g., Amadori et al., 2018; Csanady, 1977; Rao & Murthy, 2001; Wang et al., 2000).

Upwelling in large lakes has mainly been studied during the strongly stratified summer period, when it is associated with nearshore-offshore exchange (McKinney et al., 2018; Valipour et al., 2019), cross-shore thermal variability (Troy et al., 2012), increased horizontal and vertical mixing (Rao & Murthy, 2001), flushing of harbor embayments (Hlevca et al., 2018), and nutrient and phytoplankton transport (Corman et al., 2010). In Lake Geneva, Ekman-type upwelling appears to be relevant for spatiotemporal heterogeneity of surface phytoplankton during the summer period (Bouffard et al., 2018; Soulignac et al., 2018). Upwelling is therefore generally considered ecologically beneficial. However, in some cases, upwelling of deep, anoxic waters can lead to a deterioration of the surface water quality and even fish kills, for example, Lake Erie, whose deep waters regularly undergo severe hypoxia (Jabbari et al., 2019; Rao et al., 2014).

On the other hand, wind-driven Ekman-type coastal upwelling during the weakly stratified winter period has received little attention, even though it is under these conditions that wind stress effects can penetrate the deepest into the water column and consequently can "lift" very deep water masses up to the surface layers. Schladow et al. (2004) reported on an extraordinary large upwelling event in Lake Tahoe (max. depth 500 m) in winter lasting for 4 days, observed by means of in situ measurements and surface temperatures deduced from satellite imagery. They concluded that the amplitude of the upwelling covered the full water depth and affected 50% of the lake's surface. Although this was considered an extraordinary event, their findings vividly illustrate the potential role of wintertime coastal upwelling in affecting the hypolimnetic dynamics in large, deep lakes.

In the present study, we aim to investigate the as yet little-known dynamics of wintertime coastal upwelling and address the following questions: (i) Does Ekman-type coastal upwelling occur in Lake Geneva, Western Europe's largest lake during the weakly stratified winter period? (ii) If so, can it provide an efficient pathway for hypolimnetic-epilimnetic exchange under favorable wind conditions? And thus, (iii) does it contribute to deepwater renewal and reoxygenation in the deep hypolimnion? To achieve this,

we combined detailed field observations, three-dimensional (3-D) numerical modeling, and model-based Lagrangian particle tracking.

The paper is organized as follows: The characteristics of Lake Geneva, the observational data, the 3-D numerical model, and the particle tracking algorithm are described in section 2. In section 3, the prevailing thermal stratification and meteorological data are introduced. Field observations and hydrodynamic model results are presented and analyzed, and the origin and fate of upwelled deepwater masses are determined based on Lagrangian particle tracking results. The results and their implications are discussed in section 4, followed by the conclusions in section 5. A supporting information (SI) section provides additional clarifications/details on certain topics mentioned in the text.

2. Materials and Methods

2.1. Study Site Lake Geneva

Located between Switzerland and France, Lake Geneva (local name: *Lac Léman*) is often considered the birthplace of limnology (Forel, 1892) and is Western Europe's largest lake. Lake Geneva is crescent shaped and consists of two basins: a small, narrow western basin called the *Petit Lac*, with a maximum depth of 75 m, and a large eastern basin called the *Grand Lac*, with a mean depth of 170 m and a maximum depth of 309 m (Figure 1a). The lake has a surface area of 580 km^2, a length of 73 km along its major axis, and a maximum width of 14 km and is classified as warm monomictic. The shallow *Petit Lac* basin regularly destratifies every winter. The deep *Grand Lac* basin of Lake Geneva, however, remains (thermally) stratified during most years, with a thermocline typically in the range of 100–150 m depth during winter cooling and complete vertical destratification only occurring during severely cold winters (CIPEL, 2019).

Full depth profiles taken by the Commission Internationale pour la Protection des Eaux du Léman (CIPEL) on 21 December 2017, prior to the coastal upwelling event investigated in this study, show DO concentrations of 6 mg L^{-1} at 200 m depth, decreasing to approximately 3 mg L^{-1} at the bottom (CIPEL, 2019). The ventilation of these deep layers is generally attributed to complete vertical overturning due to convective cooling during severely cold winters. Recently, it was shown (Lemmin, 2020) that (i) in cold winters, vertical DO profiles with a pronounced minimum in the bulk water of the deep hypolimnion persisting for several months and higher DO concentrations toward the lake bottom occur, suggesting the lateral advection of oxygen-rich water along the lakebed; (ii) a significant spatial variability of the DO concentrations in the near-bottom layer exists as revealed by measurements taken along submarine dive tracks across the central 300 m deep plateau in the *Grand Lac* basin; and (iii) an increase in DO levels at the deepest point of the lake (309 m) can be observed every year, even during mild winters with incomplete vertical convective mixing. Field measurements (Giovanoli, 1990) indicate that dense, sediment-laden turbidity currents from the lake's main tributary, the Rhône River, occasionally reach the deepest layers. However, due to the limited frequency and intensity of these events, their contribution to deepwater renewal can be considered minor. Altogether, there is strong evidence suggesting that deepwater renewal in Lake Geneva is not only governed by vertical convective mixing but also, to some extent, by 3-D processes such as differential cooling or wind-driven coastal upwelling.

River throughflow is small, leading to a flushing time (also referred to as theoretical residence time in the literature; Monsen et al., 2002) of approximately 11 years (CIPEL, 2019). The inertial period at the latitude of Lake Geneva is approximately 16.5 hr. Numerous observational and numerical studies have shown that Coriolis force effects play an important role in determining the lake's hydrodynamics (e.g., Bauer et al., 1981; Bouffard & Lemmin, 2013; Cimatoribus et al., 2018, 2019; Lemmin, 2020; Lemmin et al., 2005).

Lake Geneva is subject to a variety of winds (local fishermen distinguish over 20 different winds by name) generated by differential heating, pressure differences across the Alps, and/or large-scale atmospheric pressure gradients (Bohle-Carbonell, 1991). The channeling effect created by the surrounding topography, that is, the Jura and Alp mountains, guides two strong, dominant pressure-gradient winds over most of the lake surface, namely, the *Vent*, blowing from the southwest, and the *Bise*, from the northeast (Figure 1a). These winds are fairly homogenous in space and steady in time for several days, typically reaching wind speeds between 5 and 15 m s^{-1} (e.g., Lemmin et al., 2005; Lemmin & D'Adamo, 1996). Both have a long fetch and are almost aligned with the shore of the western and central parts of the *Grand Lac* basin, which in

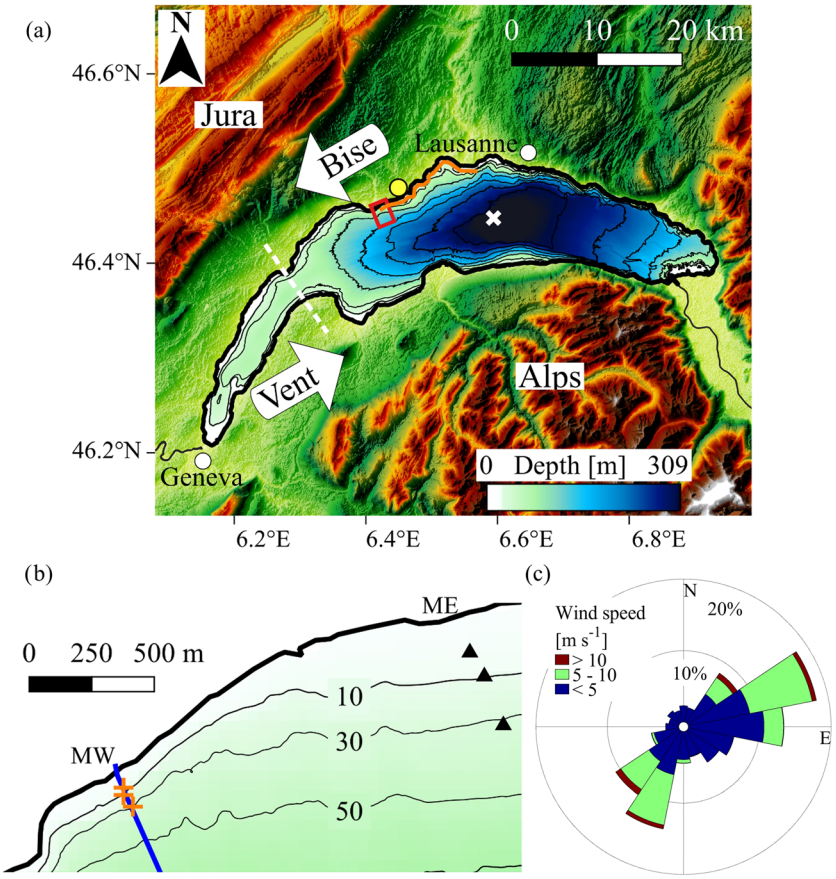

Figure 1. (a) Bathymetric map of Lake Geneva including the surrounding topography. The Jura and Alp mountains create a wide "corridor" through which two strong, dominant winds, namely, the *Vent* from the southwest and the *Bise* from the northeast, blow over most of the lake surface. The white dashed line approximately delimits the two basins, that is, the small *Petit Lac* and the large *Grand Lac*. Full-depth temperature profiles were taken at CIPEL station SHL2 (white X; depth 309 m). Meteorological data were recorded at the MeteoSwiss St. Prex station (yellow circle). The red rectangle and orange line in (a) show the study site location and the alongshore extent of the particle tracking seeding area (for details, see section 2.4), respectively. Depth is given in meters in the colorbar legend and by the isobath contours (25, 50, 100, 150, 200, 250, and 300 m). (b) Close-up of the study site during winter 2017/2018 giving an overview of the western (MW1, MW2, and MW3; orange crosses) and eastern (ME1, ME2, and ME3; black triangles) mooring sites. The blue line shows the first 500 m of the DTS fiber-optic cable. (c) Wind rose depicting the prevailing mean wind directions and strength during the observation period (1 December 2017 to 31 March 2018) recorded at the nearby meteorological station (yellow circle in a).

turn favors the development of upwelling events. The coastal upwelling on the northern shore investigated in this study is generated under *Vent* wind conditions.

2.2. Field Observations

A field measurement campaign was carried out at two sites, hereinafter referred to as western (MW1, MW2, and MW3) and eastern (ME1, ME2, and ME3) moorings during the winter of 2017/2018 near the northern shore of Lake Geneva, 20 km west of Lausanne (Figures 1a and 1b). The western mooring site had three vertical thermistor lines with a total of 34 temperature loggers (RBRsolo T and Seabird SBE-56) that were deployed from December 2017 to April 2018 at 5 m (MW1), 10 m (MW2), and 30 m depths (MW3). The moorings were aligned along a transect perpendicular to the shoreline. The 30 m depth mooring (MW3) was additionally equipped with an Acoustic Doppler Current Profiler (ADCP) (Nortek Signature 1000).

A similar set of three moorings, ME1, ME2, and ME3, was deployed 1.5 km east of the western mooring site, at the same depths. Current velocities at the 30 m depth mooring (ME3) were recorded by a combination of a

Table 1
Details of the Deployed Moorings

Moorings	Depth (m)	Instruments and settings
MW1	5	4 RBRsolo T, vertical spacing 1 m
MW2	10	15 RBRsolo T, vertical spacing 60 cm
MW3	30	12 RBRsolo T, 3 Seabird SBE-56, vertical spacing 1–3 m; Nortek Signature 1000: 26 bins of 1 m, 2 min averaging interval, 10 min measurement interval
ME1	5	4 RBRsolo T, vertical spacing 1 m
ME2	10	15 RBRsolo T, vertical spacing 60 cm
ME3	30	12 RBRsolo T, 3 Seabird SBE-56, vertical spacing 1–3 m; Nortek Aquadopp HR Profiler: 18 bins of 15 cm, 90 s averaging interval, 5 min measuring interval; Teledyne RDI Workhorse Sentinel (300 kHz): 12 bins of 2 m, 20 min averaging/measurement interval

Teledyne RDI Workhorse Sentinel (300 kHz) and a Nortek Aquadopp-HR Profiler that was added to resolve the near-bottom currents within the blanking distance (approximately 4 m) of the RDI instrument.

All thermistors had an accuracy of ±0.002°C and sampled every 2–5 s. Prior to analyzing the data, 10 min moving averages were applied to all temperature measurements. The accuracy of all current velocity measurements was in the order of 0.5 cm s^{-1}. To facilitate the comparison between the two mooring sites, the current coordinate systems were rotated to be aligned with the orientation of the local shoreline (alongshore, positive to the east; cross-shore and upslope, positive to the north) and are given as "flowing toward." Details of the mooring configurations and the instrument settings are summarized in Table 1.

In addition to the moored temperature and current instruments, near-bottom water temperatures at the western mooring site were obtained from a 1.8 km-long fiber-optic Distributed Temperature Sensing (DTS) system (Selker et al., 2006; van de Giesen et al., 2012). The DTS system measured temperatures along a fiber-optic cable that was laid down on the lakebed perpendicular to the shoreline, starting at the shore, with spatial and temporal resolutions of 1 m and 0.1°C, respectively (Figure 1b). Knowing the approximate position of the cable and the local bathymetry, we mapped distances along the cable to the corresponding depths.

Wind speed and direction were recorded every 10 min at a meteorological station at St. Prex operated by the Swiss National Weather and Climate Service (MeteoSwiss), located approximately 3 km east of the study site (Figure 1a). Hourly moving averages were applied to the meteorological data prior to the analysis. The data sets were complemented by CTD (conductivity-temperature-depth) profiles taken on a regular basis at the deepest point of the lake (SHL2 in Figure 1a) by CIPEL (CIPEL, 2019), which monitors water quality in Lake Geneva (Rimet et al., 2020).

2.3. Hydrodynamic Model

To simulate the hydrodynamics of Lake Geneva, we employed a hydrostatic version of the MITgcm, which solves an incompressible Boussinesq form of the 3-D Navier-Stokes equations (Marshall et al., 1997). This code is widely used in the oceanographic community and has successfully been applied to lakes (Djoumna et al., 2014; Dorostkar et al., 2017; Dorostkar & Boegman, 2013), and recently to Lake Geneva (Cimatoribus et al., 2019, 2018). Following Cimatoribus et al. (2018), we ran a low-resolution (LR) and a high-resolution (HR) version of the 3-D model.

The LR model (curvilinear grid, horizontal resolution 173–260 m, 35 z layers, integration time step 20 s) was initialized from rest on 15 December 2016 at 12:00 (local time) with a horizontally homogenous temperature initial condition, derived from the temperature profile at SHL2 on that date. The LR model was run until 25 October 2017, 00:00.

The interpolated 3-D temperature field from the LR model served as initial condition for the HR model, which was started from rest on 25 October 2017 at 00:00 and was run for 5 months. The HR model adopted a Cartesian grid with a constant horizontal resolution of 113 m, 50 size-varying z layers (30 cm at the surface, 10 m at the deepest point), and an integration time step of 8 s. The starting date for the HR model was selected such that the preceding days were characterized by calm wind conditions, allowing the model to

adjust to the initial conditions. Both model versions were forced at the free surface by the output of the COSMO-1 numerical weather model provided by MeteoSwiss covering the lake surface with a 1.1 km grid. We used the assimilated outputs (called reanalysis data), based on observational data, rather than pure forecast data (Voudouri et al., 2017). Quadratic bottom drag and free-slip conditions at the lateral boundaries were employed in all cases.

The model configurations were adapted from Cimatoribus et al. (2018) and Cimatoribus et al. (2019). The former study describes the configurations in detail and provides an in-depth model validation using (i) temperature and current velocity time series, and vertical temperature profiles, both recorded at a number of monitoring stations and moorings located around the entire lake, and (ii) temperature variance and kinetic energy spectra. In Figure S1, the temperature profile measured at SHL2 approximately 1 month after the beginning of the HR modeling is compared with the one obtained by the numerical model for that day. Good agreement is found.

2.4. Particle Tracking

Lagrangian particle tracking is used for analyzing the velocity output of lake or ocean circulation models. van Sebille et al. (2018) presented the fundamentals of the Lagrangian analysis, code availability, and a variety of applications in the ocean. When combined with 3-D numerical modeling, it can identify preferential transport pathways and determine the origin (backward tracking) and fate (forward tracking) of upwelled water masses in coastal regions of the ocean. In this context, particle tracking has been applied on seasonal/regional scales (e.g., Rivas & Samelson, 2011; Viglione & Thompson, 2016) and for long-term global ocean circulation studies with time scales in the order of 100 years (Tamsitt et al., 2017). Recently, Amadori et al. (2018) used particle tracking to study transport processes in Lake Garda (Italy) and found that Ekman-type coastal upwelling/downwelling along the steep shores of the lake resulted in large vertical displacement of particles, that is, water masses.

The particle tracking code employed in this study uses the method described by Döös et al. (2013), whereby particle trajectories are calculated based on the 3-D velocity field output from a hydrodynamic model, applying linear interpolation in time (between model outputs) and space (between grid points). Cimatoribus (2018) implemented the algorithm using the Python language and validated it against the analytical results discussed by Döös et al. (2013). The code was recently applied to Lake Geneva in an investigation of the dispersion of water originating from the lake's main tributary, the Rhône River (Cimatoribus et al., 2019).

Here, we used particle tracking to determine the pathways followed by hypolimnetic water masses during a 10 day coastal upwelling in January 2018. Particles were continuously released during the first 3 days (hereinafter referred to as active upwelling phase) at every grid point of the upper 15 m of the water column in an approximately 13 km alongshore by 1.5 km cross-shore nearshore region surrounding our study site (Figures 1a and S2). The seeding region was chosen based on the maximum alongshore extent of the surface temperature anomalies computed by the hydrodynamic model during the upwelling period. The origin and fate of upwelled water masses were investigated employing backward and forward tracking, respectively, and filtering the trajectories by initial and final depths.

The computed particle trajectories were used to estimate the time that particles spend in the upper layers of the water column, before descending back to greater depths. This surface exposure time has ecological implications, since it represents the time that water masses spend in contact with the atmosphere and are thus subject to heat and gas exchange.

The sensitivity of the analysis to the number of released particles was tested by varying the seeding interval between 0.5 and 2 hr, yielding between 230,000 and 890,000 particles in total. Since we were interested in the deterministic advection of water masses resolved by the hydrodynamic model, diffusion (e.g., in the form of random particle displacements) was not considered.

3. Results

3.1. Thermal Stratification of Lake Geneva

Figure 2 shows the temperature profile taken by CIPEL at SHL2 on 21 December 2017. At that time, that is, 3 weeks before the upwelling event investigated in this study, a weak thermocline remained between 75 and

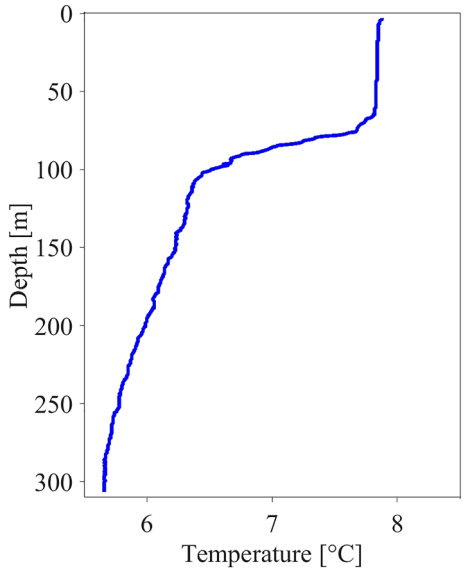

Figure 2. Temperature profile taken at the SHL2 station on 21 December 2017. For station location, see Figure 1a.

100 m. The following 3 weeks were characterized by rather mild air temperatures (T_{mean} = 5.2°C). Therefore, this profile will be considered representative for the stratification conditions during the coastal upwelling period investigated here.

3.2. Meteorological Data

Prevailing measured wind speeds and directions from 1 December 2017 to 31 March 2018 are displayed in the wind rose in Figure 1c. Wind directions in degrees refer to the direction the wind originates from. *Vent* events, which may generate coastal upwelling along the northern shore of Lake Geneva, occurred during 25% of the time. The *Vent* event analyzed in this study lasted from 16 to 26 January 2018. Wind speed and direction for that period are shown in Figures 3a and 3b, respectively. The wind blew steadily in a north-easterly direction for 7.5 days with maximum wind speeds exceeding 16 m s^{-1} and a mean value of 7.2 m s^{-1}. The two-dimensional (2-D) wind field over the lake derived from COSMO-1 data, and typical for most of that period, showed a spatially relatively homogenous wind blowing parallel to the main axis of the central part of the lake (Figure 4), thus generating favorable conditions for coastal upwelling at our study site.

3.3. Temperature and Current Moorings

The *Vent*-induced upwelling was seen at all moorings. The time series of selected DTS temperatures between 35 m depth and the end of the cable (130 m depth) are shown in Figure 5. Prior to this full coastal upwelling event, a temperature difference of less than 0.1°C between 35 and 75 m depth and a stronger change in temperature between 75 and 100 m depth indicate a thermocline depth between 75 and 100 m, in good agreement with the SHL2 profile from 21 December 2017 (Figure 2). Starting on 16 January at 00:00 at approximately 7°C, temperatures at 35, 50, and 75 m depths suddenly dropped by 0.6°C within the first 6 hr. This sudden temperature drop was most likely caused by the alongshore advection of cold water masses that underwent upwelling further west, as suggested by the dominant eastward alongshore currents at this

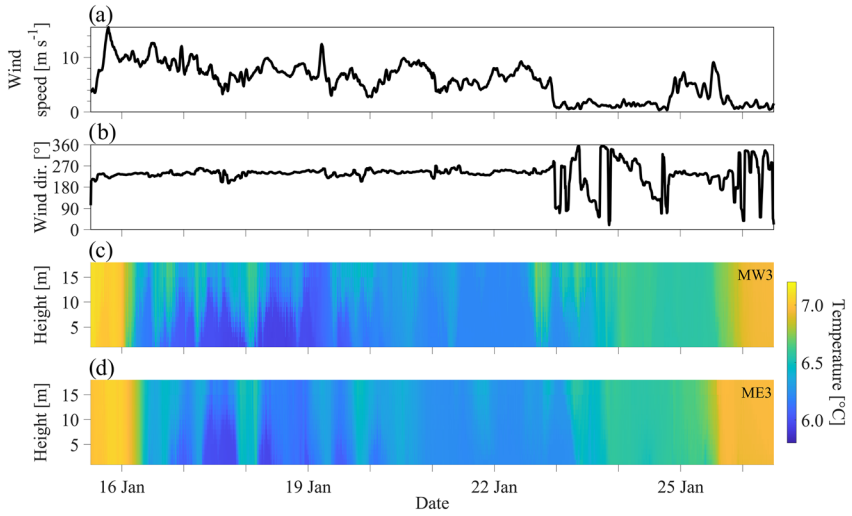

Figure 3. (a) Wind speed and (b) wind direction, both recorded during the upwelling period by the MeteoSwiss station at St. Prex. (c) and (d) Contour plots of the temperature time series recorded at the 30 m moorings MW3 and ME3, respectively. The colorbar gives the water temperature. Height is indicated in meters above the lakebed. The dates on the horizontal axis refer to the year 2018. See Figure 1 for station and mooring locations.

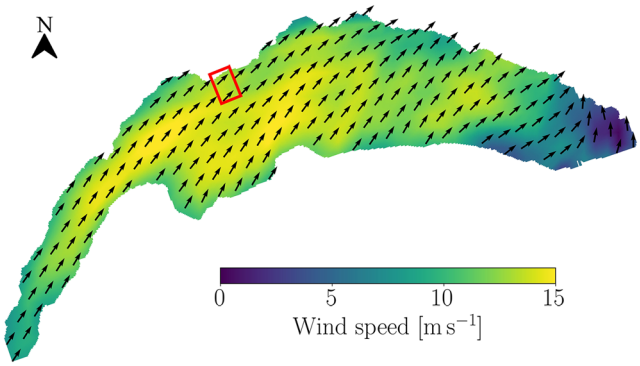

Figure 4. Two-dimensional (2-D) wind field during the upwelling event on 16 January 2018 at 12:00 (local time) derived from the COSMO-1 meteorological model. The normalized black arrows show a northeasterly wind direction (*Vent*) over most of the lake. The red rectangle marks the area where the moorings were deployed (Figure 1b). The colorbar gives the wind speed. For clarity, not all wind vectors are shown.

time (discussed below). The arrival of the upwelled cold water mass lagged behind the peak in wind speed by approximately 12 hr.

All DTS temperatures then gradually decreased further to below 6°C on 18 January at around noon (Figure 5). This period will be considered the "active upwelling" phase. The temperature pattern suggests that during that period, cold hypolimnetic water masses were continuously transported to the nearshore region by wind-driven Ekman-type coastal upwelling. During the following week, wind speeds progressively decreased, and temperatures slowly rose to approximately the values recorded before the upwelling. The minimum temperature of 5.71°C recorded at the end of the DTS cable during the upwelling period (Figure 5; 130 m depth) corresponds to the water temperature at a depth of approximately 270 m at the SHL2 station on 21 December 2017 (Figure 2), suggesting that, albeit not having reached the surface, even the deepest layers of the lake were affected by this upwelling.

Prior to the *Vent* event, all 68 thermistors at the eastern and western mooring sites showed similar temperatures within a range of 0.05°C, illustrating vertical and horizontal well-mixed conditions (Figures 3c and 3d). Following the onset of the *Vent* event, nearshore temperatures at all instruments first suddenly dropped, then remained low during the active upwelling phase, and finally began to gradually increase toward the end of the upwelling period. This time development corresponds to the one seen in the DTS recording (Figure 5). The time series of near-bottom temperatures measured by the bottommost thermistor of the mooring MW3 agreed well with the temperatures recorded at the nearby DTS system at 35 m depth (Figure 5, black line). During the active upwelling phase, several short events of warming are evident, some reaching down to the lakebed. These coincide with the peaks in the 35 m temperature record of the DTS (Figure 5) and will be further analyzed in section 4.1.

During the upwelling period, a weak stratification of less than 0.5°C often remained between the top- and bottom-most thermistors at the 30 m (Figures 3c and 3d) and 10 m depth moorings (Figure S3). Temperatures at the 5 m depth moorings were essentially vertically uniform (root mean square error, RMSE, between the bottommost and topmost thermistor signal was 0.02°C) and were close to the ones observed at the topmost thermistors at the 10 and 30 m moorings, respectively. A minimum temperature of 5.93°C was observed 1 m above the lakebed at MW3. This temperature is close to the lowest temperature recorded by the DTS (Figure 5) and corresponds to values found below depths of 200 m, as indicated by the temperature profile at SHL2 for 21 December 2017 (Figure 2).

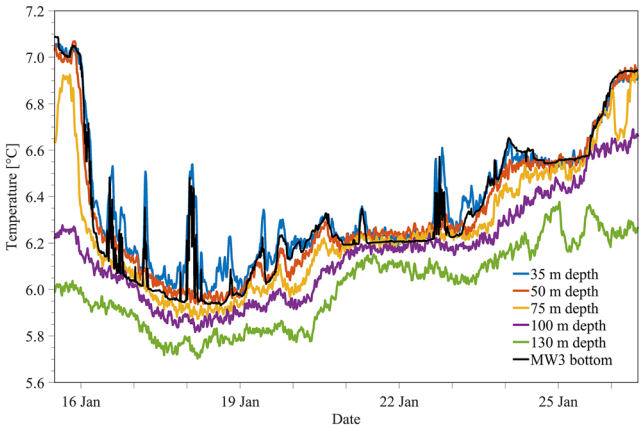

Figure 5. Temperature time series recorded by the DTS system at the western mooring site, between 30 and 130 m depth. The depth was estimated by using the approximate position of the cable and a map of the local bathymetry (Figure 1). The temperatures recorded at the bottom of the nearby MW3 mooring (30 m depth) are also shown. The different depths are given in the legend. The dates on the horizontal axis refer to the year 2018.

Figure 6 shows the observed current velocities at MW3 and ME3 during the 3 day active upwelling phase as current roses. To illustrate the prevailing processes, the water column was divided into (i) an upper layer that is >15 m above the lakebed and (ii) a lower layer that is <8 m above the lakebed. The mean values over the 3 day period are displayed for each layer. At both mooring sites, northeastward alongshore currents (i.e., aligned with the mean wind stress) dominated over the entire water column, with maximum values exceeding 25 cm s^{-1} in both layers. The gradually decreasing water temperatures during the first 3 days (Figure 5) could be explained by episodic cross-shore, upslope currents seen in the bottom layers of both moorings that carry cold water masses from the hypolimnion toward the shore, particularly at the western mooring site (Figures 6c and 6d). The observed spatial heterogeneity of the current speeds between the two moorings is likely due to a combination of effects, including the spatially varying wind velocity (Figure 4), shoreline irregularities close to the western study site, and differences in the bed slope (Figure 1b).

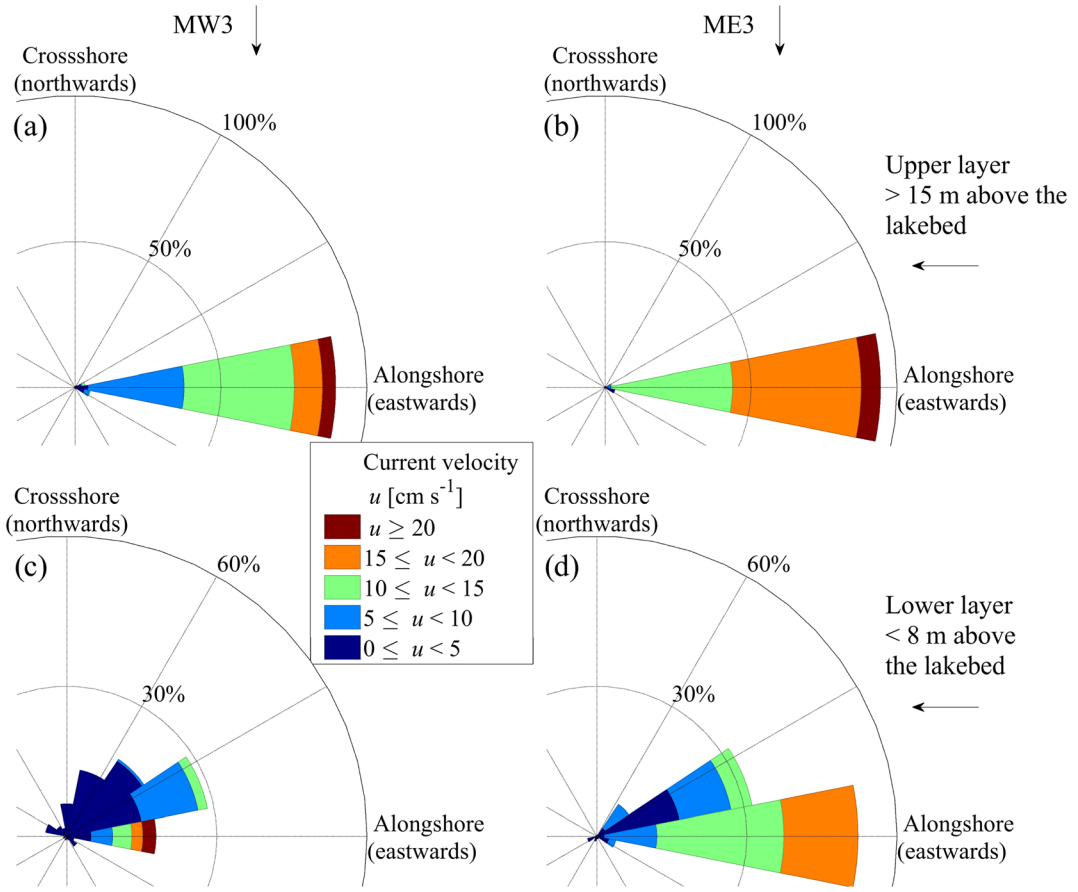

Figure 6. Current roses at MW3 (left panels) and ME3 (right panels) for the upper (a, b) and the lower (c, d) layers during the active upwelling phase from 15 January, 15:00 (onset of *Vent* event), to 18 January 2018, 12:00 (end of active upwelling phase). Current vectors were projected onto the local alongshore axis. Note that the scales in the top and bottom panels are different.

3.4. Model Results

Figure 7 shows the vertical average of the temperature signal in the lower layer of the water column (approximately between 2 and 8 m above the lakebed) recorded at mooring ME3 (blue) and computed by the HR model (red) from 13 to 28 January 2018. Due to the discretization of the bathymetry, the depth in the HR model at this location is approximately 26 m. Even though the model grid is too coarse to resolve all the details of this complex nearshore bathymetry, the model overall reproduces the upwelling event well in terms of absolute temperatures and temporal variability, and the modeled temperatures are in good agreement with field observations (RMSE approximately 0.2°C). The initial rapid temperature drop due to northeastward alongshore advection of previously upwelled cold water masses and the gradual temperature increase during the relaxation phase are both captured by the model. Furthermore, field observations and numerical modeling results show several significant temperature peaks during the active upwelling phase. These were due to temporary downwelling close to the shore and are discussed in section 4.1. The overall agreement between observational data and numerical modeling results allowed us to investigate further the 3-D structure of the upwelling. It should

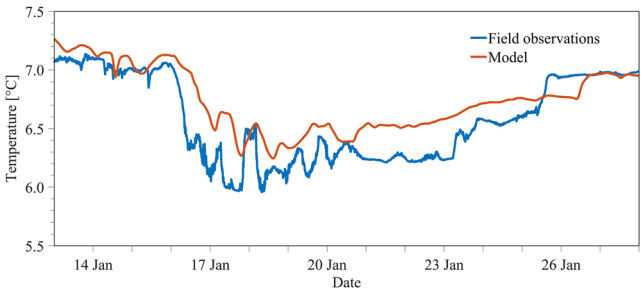

Figure 7. Temperature time series in the lower layer of the water column (approximately 2 to 8 m above the lakebed) as recorded at ME3 (blue) and as computed by the high-resolution (HR) model (red). The dates on the horizontal axis refer to the year 2018.

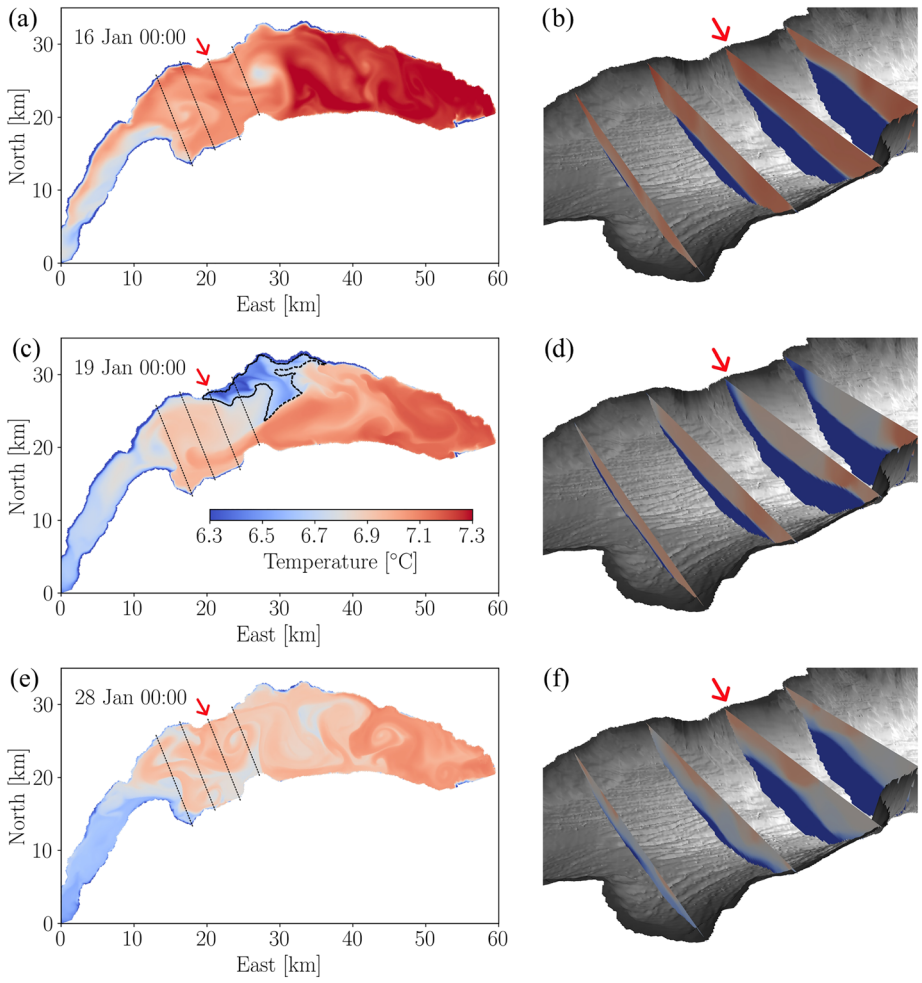

Figure 8. Modeled near-surface temperatures (a, c, e) and vertical full-depth temperature slices at selected locations (b, d, f) before (16 January 2018, 00:00), during (19 January 2018, 00:00), and after (28 January 2018, 00:00) the upwelling period. The locations of the vertical slices are marked in the surface contour plots by the black lines. The red arrow indicates the mooring sites. The colorbar in (c) gives the temperature range for all panels.

be emphasized that this would not have been possible by only using the point measurements of the field observations.

Maps of the modeled near-surface temperatures at 1 m depth before (16 January 2018, 00:00), during (19 January 2018, 00:00), and after (28 January 2018, 00:00) the upwelling period, as well as vertical temperature slices at selected locations, are displayed in Figure 8. In order to estimate the surface area affected by this event, we considered the surface temperature anomaly (i.e., local surface temperatures minus basin-wide averaged surface temperature) as a proxy for upwelled water masses. By assuming that the upper layer was well mixed before the onset of the *Vent* event (Figure 3), a surface temperature anomaly of −0.2°C indicates that these surface water masses originated from well within the thermocline (75–100 m depth; Figure 2). The modeling results suggest that, based on this choice of threshold, an area of up to 50 km^2 was affected by the upwelling (black contoured area in Figure 8c). This corresponds to approximately 10% of the surface area of the *Grand Lac* basin. It should be noted that comparably lower surface temperatures in some parts of the lake prior to the *Vent*-induced upwelling (Figure 8a) were not related to coastal upwelling. Instead, they could be attributed to (i) differential cooling of the shallow *Petit Lac* basin and shallow nearshore regions of the *Grand Lac* and (ii) a counterclockwise rotating gyre in the central part of the *Grand Lac*. Upwelling in the center of the gyre resulted in a local dome-shaped thermocline (easternmost slice in Figure 8b) and was a remnant of a previous wind event.

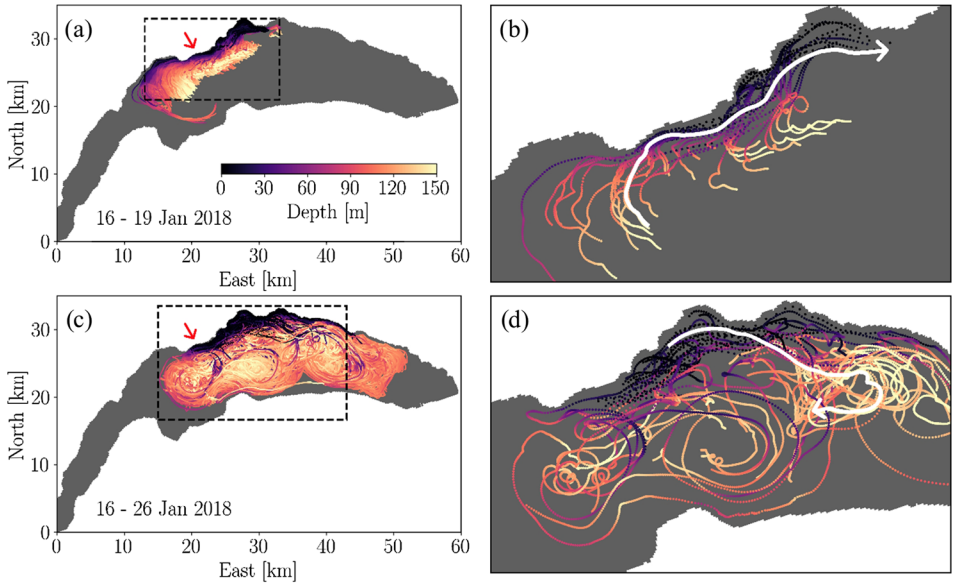

Figure 9. (a) Backward tracking (from 19 to 16 January) and (c) forward tracking (from 16 to 26 January) of particles during the upwelling event from 16 to 26 January 2018. For better visualization, a random subset of 10,000 particles was selected prior to plotting. (b and d) Close-ups of the areas delimited by the black dashed lines in (a) and (c) showing, respectively, backward and forward tracking with a random subset of 30 particles. The white arrows indicate the traveling direction of the released particles along one exemplary trajectory, reflecting the movement of water parcels. The swirling motions in panel (d) are due to large-scale gyres. Particles were continuously released in the nearshore study site (marked by the red arrow) within the upper 15 m of the water column (section 2.4). Only particles with an origin depth (backward tracking) or a final depth (forward tracking) of more than 100 m are displayed, and all trajectories shown in (d) end on 26 January. Particle depth is given in the colorbar legend in (a). Note that the size of the areas in panels (b) and (d) is different.

Vertical temperature slices at selected locations on 19 January 2018 at 00:00 (Figure 8d) revealed a significant tilt of the thermocline perpendicular to the wind stress and thus are in agreement with our field measurements above, indicating that the cold temperatures observed near the northern shore were due to a full upwelling event (i.e., the thermocline reached the surface). The shape of this modeled transect across the lake illustrates the tilting and surfacing of the thermocline that was generated by a sufficiently strong and long-lasting *Vent* wind event. The shape was confirmed experimentally by north-south CTD transects in this part of the lake taken during a similar coastal upwelling event in December 2018 (Figure S4).

3.5. Particle Tracking Results

Observed and modeled temperatures near the northern shore of the lake show that water masses from far below the thermocline reached the nearshore surface, confirming that wintertime coastal upwelling is an effective transport process for hypolimnetic-epilimnetic water exchange. To further assess the upwelling pathways, that is, the origin and fate of the upwelled water masses in our study area, we employed backward and forward particle tracking. The computed Lagrangian trajectories with an origin (backward tracking) or final (forward tracking) depth below the thermocline (i.e., 100 m depth) were calculated for a total of approximately 230,000 released particles. Doubling (tripling) the number of released particles by reducing the seeding interval by a factor of 2 (3) did not change the results of the particle trajectory analysis, thus indicating their statistical robustness. For better visualization, random subsets of 10,000 (Figures 9a and 9c) and 30 (Figures 9b and 9d) particles are shown. Figure S5 shows all 230,000 particle trajectories for both backward and forward tracking.

The analysis of the backward tracking trajectories revealed that approximately 30% of all particles released near the shore between 0 and 15 m depth during the active upwelling phase originated from the hypolimnion. The maximum computed origin depth of approximately 200 m is in good agreement with our field observations. Likewise, forward particle tracking confirmed that a similar fraction of the particles released

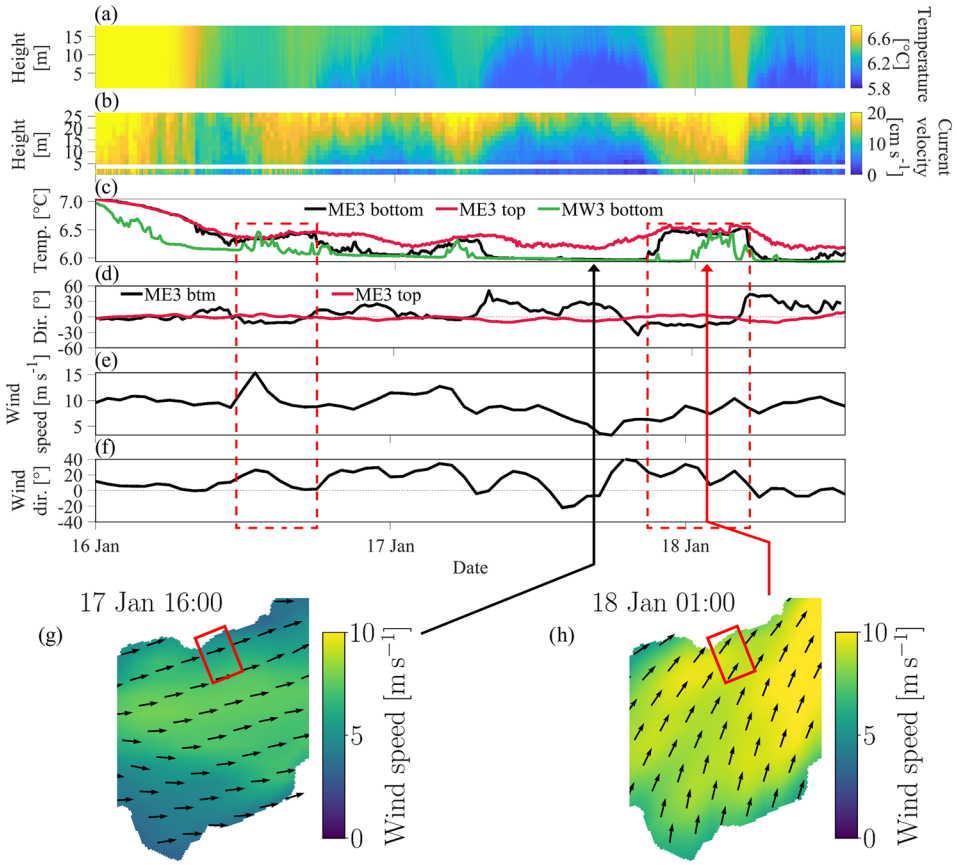

Figure 10. (a) Contour plot of the temperature recorded at ME3 during the active upwelling phase. (b) Contour plot of the current velocity recorded at ME3; height is given in meters above the lakebed. (c) Temperature time series recorded at ME3 and MW3 for selected heights. The temperatures of the bottom-most and topmost thermistors, respectively (MW3 btm: 0.3 m; ME3 btm: 1 m, top: 18 m above the lakebed) are given. (d) Median-filtered current direction recorded at ME3 in the lower (<10 m height; black curve) and upper (>15 m height; red curve) part of the water column. (e and f) Wind speed and direction derived from the COSMO-1 meteorological model and spatially averaged over the red rectangle shown in (g) and (h). Current (and wind) directions are expressed as divergence from the alongshore direction: 0° corresponds to an eastward alongshore flow (wind), and positive numbers reflect a shift in the current (wind) direction toward cross-shore and upslope (onshore). The dates on the horizontal axis refer to the year 2018. (g and h) Two-dimensional COSMO-1 wind field on 17 January at 16:00 (active upwelling) and 18 January at 01:00 (downwelling), respectively. The corresponding measured current velocity profiles are shown in Figure 11. The red rectangles in (g) and (h) indicate the areas where the moorings were deployed. Red dashed-line rectangles in (c)–(f) mark downwelling events. Temperature, current velocity, and wind speed are given in the colorbar legends.

near the shore descended back down into the hypolimnion after wind stress ceased, reaching a maximum depth of more than 200 m.

A clear difference can be seen in the particle motion pattern of the upward motion during the initiation of upwelling and downward motion during the relaxation period (Figure 9). As would be expected, most of the upward motion of the deep waters is generated over the lateral slope in close proximity to the nearshore upwelling zone (Figures 9a and 9b). In contrast, the trajectories of the downward motion spread out over a much wider region covering a large portion of the *Grand Lac* basin (Figures 9c and 9d). Furthermore, when tracking only a limited number of particles (Figure 9d), it becomes obvious that a significant number of them are entrained into the large-scale gyres in this area, as detailed by Cimatoribus et al. (2019). Thus, the gyre motion field provides for an efficient spreading of the oxygen enriched water masses that originated in the 15 km-long nearshore zone of our study site within most of the *Grand Lac* basin.

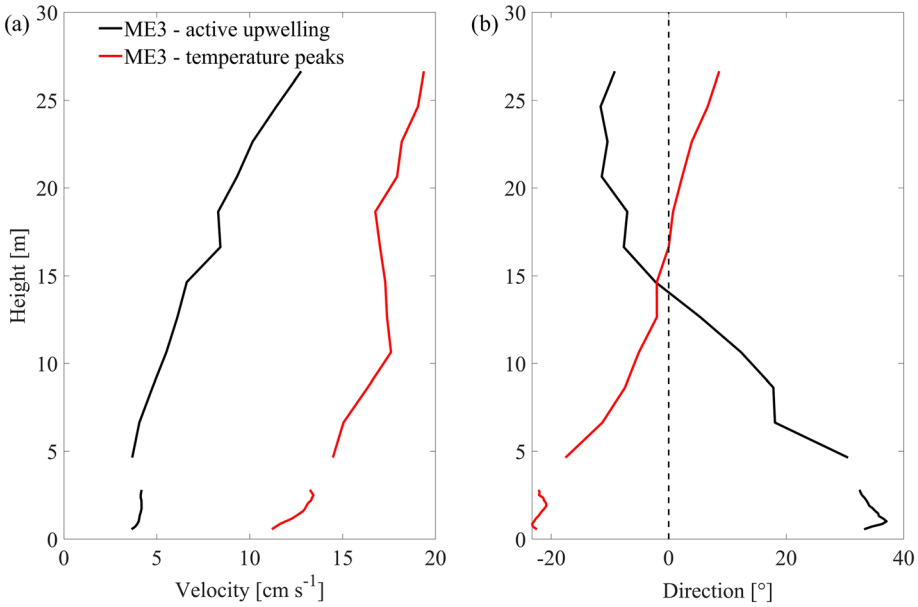

Figure 11. Profiles of (a) current velocity and (b) current direction, both recorded at mooring ME3. The profiles are representative for periods of downwelling related to the observed temperature peaks (red curves) and active upwelling (black curves). The corresponding times are marked in Figure 10 by the long red and black arrows. Current directions are plotted as divergence from the alongshore direction: 0° corresponds to an eastward, alongshore flow, and positive values reflect a shift in the current direction toward cross-shore and upslope. Height is given in meters above the lakebed.

4. Discussion

4.1. Observed Temperature Peaks Near the Shore During the Active Upwelling Phase

Coastal upwelling of cold hypolimnetic water manifested itself during the active period as cross-shore upslope currents in an approximately 10 m-thick bottom boundary layer at both moorings MW3 and ME3 (Figure 6). Comparing the contour plots of water temperature and current velocities at ME3 (Figures 10a and 10b), it is evident that the two were strongly correlated, which is confirmed by normalized cross-correlation coefficients of 0.67 and 0.85 for the upper and lower layers, respectively. In particular, it can be seen that after the onset of the upwelling, events of high current velocity occur simultaneously with an increase of nearly 0.5°C in water temperature in the whole bottom boundary layer. The near-bottom temperatures overall decreased during the active upwelling phase, producing a strong gradient between the top and the bottom layer (Figures 5 and 10c). However, during this phase, the temperatures in the bottom boundary layer sporadically approached again those that were measured in the top layer (Figure 10c). This suggests that warm near-surface waters descended down to 30 m depth.

In order to determine the paths followed by these water masses, the current directions in the top and bottom layers of the eastern mooring ME3 are plotted in Figure 10d. Overall, current directions, particularly in the top layer, are oriented alongshore. However, superimposed on this long-term trend, current directions in the bottom layer are downslope-oriented during the warming events, whereas those in the top layer are pointing slightly toward the shore. This is a current pattern characteristic of downwelling where near-surface water is pushed toward the shore by the wind and then down the slope. The full-depth current profiles for this downwelling event document the flow direction reversal between the top (onshore) and bottom (offshore/downslope) layers, as well as the high velocities (red curve in Figure 11; red arrow in Figure 10). In contrast, the full-depth direction profiles measured during the active upwelling phase (black curve in Figure 11; black arrow in Figure 10) show the inverse with offshore movement in the top layer and upslope motion in the bottom layer.

An analysis of the time development of the COSMO-1 wind field over the lake in the vicinity of our study area during these downwelling events confirms that the spatially averaged wind over an area of 3 km × 3 km is oriented onshore and can therefore push warmer near-surface waters toward the shore (Figures 10e and

10f). Maps of the instantaneous wind pattern in the area confirm the change in orientation with a significant onshore component during these events when compared to the pattern when upwelling is dominant and most vectors are oriented along the shore (Figure 10g). Thus, while the general wind pattern is that of a *Vent*, causing upwelling in the nearshore area, temporal variability in the wind orientation can generate short events of downwelling (Movie S1).

In Figure 10b, the near-bottom temperature at western mooring MW3 also shows these warm water peaks at the same time, thus indicating that these downwelling events covered the full lateral extent of the study area. These peaks also coincide with the peaks seen in the DTS temperature recording at 35 m depth. The DTS near-bottom temperatures below 50 m depth, that is, further than 300 m offshore, continuously decreased and showed no sign of warmer surface water intrusions (Figure 5). This confirms the nearshore nature of these downwelling events. During these events, oxygen-saturated near-surface water is rapidly pushed to greater depths. The alternating interplay between upwelling and downwelling in this lateral boundary layer causes strong mixing in the whole area and can further increase the oxygen content of these water masses, which, as was seen in the particle-tracking analysis above (Figure 9), will eventually descend down into the deep hypolimnion. It should be noted that the numerical model reasonably well reproduced the temperature peaks (Figure 7), and thus the downwelling events, despite its limited resolution close to the shoreline.

4.2. Wintertime Coastal Upwelling as a Pathway for Deepwater Renewal

As indicated by the field observations and confirmed by Lagrangian particle tracking, hypolimnetic water from as deep as O(200 m) was transported upslope during the upwelling period. The particle tracking results also suggest that most of the water masses upwelled in the nearshore area descended back to a maximum depth O(200 m) after the wind stress had ceased (Figures 9d and S5b). The trajectories of these descending water masses were found to be strongly affected by the dynamics of the large-scale motions in the lake, often characterized by large gyres (Cimatoribus et al., 2019), as seen in Figures 9c, 9d, and S5b. Forward particle tracking shows that due to the presence of these large-scale gyres, descending particles rapidly spread over a wide area in the *Grand Lac* basin, thus demonstrating that coastal upwelling during wintertime, even in a limited nearshore area, is an effective contributor to deepwater renewal over a much larger area.

Once brought to the surface, that is, in direct contact with the atmosphere, the upwelled water is subject to heat and gas exchange. Hence, the time upwelled water masses spend near the surface appears to be of interest when considering the ecological implications of this physical process. By integrating the time that particles spent in the upper 15 m of the water column, we estimated a surface exposure time for particles with an origin and final depth below the thermocline, that is, for approximately 30% of all released particles. We found that these upwelled particles spent on average about 1 day near the surface before descending back below the thermocline. Approximately 25% of the upwelled particles spent more than 1.5 days, and the maximum observed surface exposure time was more than 5 days.

While the surface exposure time might be limited to a few days, conditions for air-water oxygen exchange are highly favorable during wintertime upwelling due to (i) high wind speeds, which cause intense mixing and large gas transfer velocities; (ii) high values of oxygen saturation concentrations at low in situ temperatures (i.e., high solubility of oxygen); and, finally, (iii) low measured in situ concentration of oxygen in upwelled hypolimnetic water (about 6 mg L^{-1} at 200 m depth). A rough, order-of-magnitude estimation of the oxygen exchange indicates a DO flux of 23 t km^{-2} day^{-1} or an oxygen injection of about 1,000 t in our study area for the conditions specified above. However, great care has to be taken when interpreting such average values (for details, see Text S1). Upwelling also occurs simultaneously in other sections of the northern shore of Lake Geneva, thus increasing the total oxygen input during the surface exposure of the deepwater masses.

Moreover, a number of other processes that may further enhance the air-water oxygen exchange estimated above take place at the same time in this near surface layer:

i. Air injection by bubbles caused by breaking or whitecapping waves increases the rate of oxygen exchange (e.g., Woolf, 1993).
ii. In addition to direct air-water gas exchange, significant turbulent mixing between upwelled hypolimnetic (low in DO) and DO-saturated epilimnetic water can be expected, considering the high levels of turbulence induced by wind stress and bottom friction in the shallow nearshore region.

iii. The nearshore downwelling events discussed in section 4.1 brought near-surface water masses down to a depth of 30–40 m, thus contributing to additional mixing.
iv. Results of the 3-D modeling indicate that the cold upwelled hypolimnetic water can spread over a large surface area. This spreading leads to an unstable stratification in the surface layer, which results in convective downward motion of these cold waters. It was previously observed that this downward motion often occurs in large size convective plumes (several meters in diameter) that have been estimated to cover up to 10% of the lake surface area (Thorpe et al., 1999) and that transport oxygen-rich surface waters into deeper layers more efficiently than small-scale turbulent mixing.

The contribution from these different processes cannot be quantified with our data. However, the total resulting DO input into the upwelled waters that will return to the deep layers is most likely substantially higher than the estimate given above.

It has to be noted that the strength of particle tracking simulations lies in their ability to identify trajectories and preferred pathways of upwelled water masses. Using particle tracking, one cannot determine the actual oxygen supply brought down to the deep layers, because particles have neither mass nor volume, and turbulent mixing between the upwelled and the surrounding waters cannot be assessed. A more robust quantification of the deep ventilation potential due to wintertime coastal upwelling, for example, by means of numerical tracers (e.g., Matsumoto et al., 2015; Sun et al., 2017), goes beyond the scope of this study.

5. Summary and Conclusions

Little is known about the physical dynamics of coastal upwelling in large lakes during wintertime. In order to investigate this transport process, we performed a detailed analysis of a full coastal upwelling event in Lake Geneva, which occurred in January 2018 due to a strong southwesterly alongshore *Vent* wind event, and that lasted for 10 days. Field observations using moored current profilers and temperature nodes near the northern shore of the lake during winter 2017/2018 combined with 3-D numerical modeling and Lagrangian particle tracking proved to be a powerful tool set that gave new insight into complex 3-D lake hydrodynamic processes on a larger scale.

Field measurements showed that during the upwelling period, water masses from as deep as 200 m, well below the thermocline, were brought to the surface in the nearshore area and transported along the shore at high velocities. At the same time, short downwelling events, caused by small directional changes in the wind field over the lake, transported warmer oxygen-saturated surface water toward the shore and down the slope. Near-bottom temperatures obtained from a DTS fiber-optic cable revealed that downwelling was limited to a depth of less than 50 m. The interplay of short downwelling events with the longer-lasting upwelling most likely causes vigorous mixing of the nearshore water masses, thus increasing the overall oxygen content.

Upwelling and temporary nearshore downwelling events were well reproduced by a 3-D hydrodynamic model (RMSE 0.2°C) and thus allowed us to investigate the effects of the observed upwelling over a wider area of the lake. It should be noted that this would not have been possible using only the point measurements of the field observations. Computed surface temperatures suggest that upwelled waters spread out over up to 10% of the surface area of the *Grand Lac*. Lagrangian particle tracking based on the modeled 3-D current velocity field confirmed that this water originated from the hypolimnion (maximum depth 200 m). Upwelled particles spend on average 1 days, and up to 5 days near the surface before descending again to the hypolimnion after the wind stress ceased. Once brought to the surface, upwelled hypolimnetic water (low in DO) is subject to gas (notably oxygen) exchange with the atmosphere. Considering the strong wind forcing and weak stratification, vigorous mixing between the upwelled hypolimnetic and DO-saturated epilimnetic water can also be expected.

Particle tracking showed that the upwelled water masses originated from a limited section of the slope in the vicinity of the study area, whereas water masses descending into the deep hypolimnion after the upwelling were caught in large-scale gyres and spread over a wide area of the hypolimnion, thus emphasizing the 3-D structure of upwelling and deepwater renewal. Both field observations and particle tracking results suggest that coastal upwelling during the weakly stratified winter period provides an efficient pathway for deepwater renewal in Lake Geneva.

During our field observations between December 2017 and March 2018, four other upwelling periods, comparable in amplitude and duration, occurred (Figure S6). Recently, a study on climate change effects in Switzerland (CH2018, 2018) reported that during their reference period (1981 to 2011), southwesterly winds (*Vent*) were the most important strong winds during winter in the Lake Geneva area. This further supports our findings that coastal upwelling produced by these winds is a significant contributor to deepwater dynamics. Historical continuous water temperature recordings from a nearshore station close to the present study site, dating back several decades, provide additional evidence that full coastal upwelling is a frequently occurring transport process during the weakly stratified winter period.

Here, we provided for the first time in Lake Geneva details of the *Vent*-generated upwelling dynamics during winter over a section of the northern shore. Water mass movements related to upwelling similar to those observed in the study area take place simultaneously over other sections of the northern shore, thus reinforcing the lakewide effect of such a *Vent* event on deepwater renewal. Moreover, *Bise* wind events blowing from the opposite direction with comparable strength, duration, frequency, and fetch also occur during winter (Figure 1c). They bring cold air from Northern Eurasia contributing to differential cooling and can produce coastal upwelling on the southern shore of the lake. Therefore, the integral effect of all these upwelling events on deepwater renewal during the weakly stratified winter season can potentially be substantial.

In the face of rising global surface water temperatures, our findings demonstrate that winter Ekman-type coastal upwelling, an overlooked transport process, could play an increasingly important role in deepwater renewal in Lake Geneva and possibly also in other large deep lakes with favorable wind conditions. It is less sensitive to climate change effects, as opposed to convective cooling, which is expected to continue weakening and thus become less efficient.

Our study has revealed that wintertime coastal upwelling in large lakes is a highly complex and transient, yet potentially significant 3-D transport process contributing to deepwater renewal. Therefore, it cannot be adequately described by traditional 1-D concepts or models. This should be taken into consideration when making long-term predictions of lake system dynamics, such as those related to climate change.

Data Availability Statement

The in situ data and model results supporting the findings of this study are available online (at https://doi.org/10.5281/zenodo.3968410).

Acknowledgments

This work was supported by the Swiss National Science Foundation (Grant No. 159422) and the Bois Chamblard Foundation. Meteorological data were provided by the Federal Office of Meteorology and Climatology in Switzerland (MeteoSwiss). Full-depth temperature and dissolved oxygen profile data were provided for station SHL2 by © OLA-IS, AnaEE-France, INRAE of Thonon-les-Bains, CIPEL. The Distributed Temperature Sensing (DTS) system was made available by Hendrik Huwald (Laboratory of Cryospheric Sciences, CRYOS, EPFL). We would like to thank Htet Kyi Wynn for assisting with the fieldwork.

References

Adrian, R., O'Reilly, C. M., Zagarese, H., Baines, S. B., Hessen, D. O., Keller, W., et al. (2009). Lakes as sentinels of climate change. *Limnology and Oceanography*, *54*, 2283–2297. https://doi.org/10.4319/lo.2009.54.6_part_2.2283

Amadori, M., Piccolroaz, S., Giovannini, L., Zardi, D., & Toffolon, M. (2018). Wind variability and Earth's rotation as drivers of transport in a deep, elongated subalpine lake: The case of Lake Garda. *Journal of Limnology*, *77*, 505–521. https://doi.org/10.4081/jlimnol.2018.1814

Ambrosetti, W., & Barbanti, L. (1999). Deep water warming in lakes: An indicator of climatic change. *Journal of Limnology*, *58*(1), 1–9. https://doi.org/10.4081/jlimnol.1999.1

Bauer, S. W., Graf, W. H., Mortimer, C. H., & Perrinjaquet, C. (1981). Inertial motion in Lake Geneva (Le Léman). *Archives for meteorology, geophysics, and bioclimatology, Series A*, *30*(3), 289–312. https://doi.org/10.1007/BF02257850

Bohle-Carbonell, M. (1991). Wind and currents: Response patterns of Lake Geneva. *Annales Geophysicae*, *9*, 82–90.

Bouffard, D., Kiefer, I., Wüest, A., Wunderle, S., & Odermatt, D. (2018). Are surface temperature and chlorophyll in a large deep lake related? An analysis based on satellite observations in synergy with hydrodynamic modelling and in-situ data. *Remote Sensing of Environment*, *209*, 510–523. https://doi.org/10.1016/j.rse.2018.02.056

Bouffard, D., & Lemmin, U. (2013). Kelvin waves in Lake Geneva. *Journal of Great Lakes Research*, *39*(4), 637–645. https://doi.org/10.1016/j.jglr.2013.09.005

CH2018 (2018). *CH2018—Climate scenarios for Switzerland, Technical Report* (p. 271). Zurich: National Centre for Climate Services. ISBN: 978-3-9525031-4-0. https://naturalsciences.ch/service/publications/107865-ch2018—climate-scenarios-for-switzerland-technical-report

Cimatoribus, A. A. (2018). C-tracker. https://doi.org/10.5281/zenodo.1034118

Cimatoribus, A. A., Lemmin, U., & Barry, D. A. (2019). Tracking Lagrangian transport in Lake Geneva: A 3D numerical modeling investigation. *Limnology and Oceanography*, *64*, 1252–1269. https://doi.org/10.1002/lno.11111

Cimatoribus, A. A., Lemmin, U., Bouffard, D., & Barry, D. A. (2018). Nonlinear dynamics of the nearshore boundary layer of a large lake (Lake Geneva). *Journal of Geophysical Research: Oceans*, *123*, 1016–1031. https://doi.org/10.1002/2017JC013531

CIPEL (2019). Rapports sur les études et recherches entreprises dans le bassin lémanique, Campagne 2018. Commission internationale pour la protection des eaux du Léman (CIPEL), Nyon, Switzerland. Retrieved from https://www.cipel.org/wp-content/uploads/2019/10/RapportScientifique_camp_2018-1.pdf, last accessed 4. December 2019.

Coats, R., Perez-Losada, J., Schladow, G., Richards, R., & Goldman, C. (2006). The warming of Lake Tahoe. *Climatic Change*, *76*(1-2), 121–148. https://doi.org/10.1007/s10584-005-9006-1

Coman, M. A., & Wells, M. G. (2012). Temperature variability in the nearshore benthic boundary layer of Lake Opeongo is due to wind-driven upwelling events. *Canadian Journal of Fisheries and Aquatic Sciences*, *69*(2), 282–296. https://doi.org/10.1139/f2011-167

Corman, J. R., McIntyre, P. B., Kuboja, B., Mbemba, W., Fink, D., Wheeler, C. W., et al. (2010). Upwelling couples chemical and biological dynamics across the littoral and pelagic zones of Lake Tanganyika, East Africa. *Limnology and Oceanography*, *55*(1), 214–224. https://doi.org/10.4319/lo.2010.55.1.0214

Cossu, R., & Wells, M. G. (2013). The interaction of large amplitude internal seiches with a shallow sloping lakebed: Observations of benthic turbulence in Lake Simcoe, Ontario, Canada. *PLoS ONE*, *8*(3), e57444. https://doi.org/10.1371/journal.pone.0057444

Csanady, G. T. (1977). Intermittent 'full' upwelling in Lake Ontario. *Journal of Geophysical Research*, *82*(3), 397–419. https://doi.org/10.1029/JC082i003p00397

Djoumna, G., Lamb, K. G., & Rao, Y. R. (2014). Sensitivity of the parameterizations of vertical mixing and radiative heat fluxes on the seasonal evolution of the thermal structure of Lake Erie. *Atmosphere-Ocean*, *52*, 294–313. https://doi.org/10.1080/07055900.2014.939824

Döös, K., Kjellsson, J., & Jönsson, B. (2013). TRACMASS—A Lagrangian trajectory model. In T. Soomere, & E. Quak (Eds.), *Preventive Methods for Coastal Protection: Towards the Use of Ocean Dynamics for Pollution Control* (pp. 225–249). Heidelberg: Springer International Publishing. https://doi.org/10.1007/978-3-319-00440-2_7

Dorostkar, A., & Boegman, L. (2013). Internal hydraulic jumps in a long narrow lake. *Limnology and Oceanography*, *58*(1), 153–172. https://doi.org/10.4319/lo.2013.58.1.0153

Dorostkar, A., Boegman, L., & Pollard, A. (2017). Three-dimensional simulation of high-frequency nonlinear internal wave dynamics in Cayuga Lake. *Journal of Geophysical Research: Oceans*, *122*, 2183–2204. https://doi.org/10.1002/2016JC011862

Ekman, V. W. (1905). On the influence of the Earth's rotation on ocean-currents. Arkiv för Matematik, Astronomi, och Fysik 2, 1–52.

Fer, I., Lemmin, U., & Thorpe, S. A. (2002). Winter cascading of cold water in Lake Geneva. *Journal of Geophysical Research*, *107*(C6), 13–1–13–16. https://doi.org/10.1029/2001JC000828

Forel, F. A. (1892). *Le Léman: Monographie Limnologique 1*. Lausanne, Switzerland: F. Rouge.

Friedrich, J., Janssen, F., Aleynik, D., Bange, H. W., Boltacheva, N., Çagatay, M. N., et al. (2014). Investigating hypoxia in aquatic environments: Diverse approaches to addressing a complex phenomenon. *Biogeosciences*, *11*(4), 1215–1259. https://doi.org/10.5194/bg-11-1215-2014

Giovanoli, F. (1990). Horizontal transport and sedimentation by interflows and turbidity currents in Lake Geneva. In M. M. Tilzer, & C. Serruya (Eds.), *Large lakes: Ecological structure and function*, *Brock/Springer Series in Contemporary Bioscience* (pp. 175–195). Berlin, Heidelberg: Springer. https://doi.org/10.1007/978-3-642-84077-7_9

Goldman, C. R., Kumagai, M., & Robarts, R. D. (Eds.) (2013). *Climatic change and global warming of inland waters: Impacts and mitigation for ecosystems and societies*. Chichester, West Sussex, UK: Wiley-Blackwell.

Hlevca, B., Wells, M. G., Cruz Font, L., Doka, S. E., Portiss, R., St. John, M., & Cooke, S. J. (2018). Water circulation in Toronto Harbour. *Aquatic Ecosystem Health and Management*, *21*(3), 234–244. https://doi.org/10.1080/14634988.2018.1500059

Homma, H., Nagai, T., Shimizu, K., & Yamazaki, H. (2016). Early-winter mixing event associated with baroclinic motions in weakly stratified Lake Biwa. *Inland Waters*, *6*, 364–378. https://doi.org/10.1080/IW-6.3.898

Jabbari, A., Ackerman, J. D., Boegman, L., & Zhao, Y. (2019). Episodic hypoxia in the western basin of Lake Erie. *Limnology and Oceanography*, *64*(5), 2220–2236. https://doi.org/10.1002/lno.11180

Lemmin, U. (2020). Insights into the dynamics of the deep hypolimnion of Lake Geneva as revealed by long-term temperature, oxygen, and current measurements. *Limnology and Oceanography*. Advance online publication. https://doi.org/10.1002/lno.11441

Lemmin, U., & D'Adamo, N. (1996). Summertime winds and direct cyclonic circulation: Observations from Lake Geneva. *Annales Geophysicae*, *14*(11), 1207–1220. https://doi.org/10.1007/s00585-996-1207-z

Lemmin, U., Mortimer, C. H., & Bäuerle, E. (2005). Internal seiche dynamics in Lake Geneva. *Limnology and Oceanography*, *50*(1), 207–216. https://doi.org/10.4319/lo.2005.50.1.0207

Likens, G. E. (Ed.) (2010). *Biogeochemistry of inland waters: A derivative of Encyclopedia of inland waters*. Amsterdam; Boston: Elsevier/Academic Press. ISBN: 978-0-12-381996-3.

Livingstone, D. M. (1993). Temporal structure in the deep-water temperature of four Swiss lakes: A short-term climatic change indicator? *Verhandlungen - Internationale Vereinigung fur Theoretische und Angewandte Limnologie*, *25*(1), 75–81. https://doi.org/10.1080/03680770.1992.11900062

Marshall, J., Adcroft, A., Hill, C., Perelman, L., & Heisey, C. (1997). A finite-volume, incompressible Navier Stokes model for studies of the ocean on parallel computers. *Journal of Geophysical Research*, *102*(C3), 5753–5766. https://doi.org/10.1029/96JC02775

Matsumoto, K., Tokos, K. S., & Gregory, C. (2015). Ventilation and dissolved oxygen cycle in Lake Superior: Insights from a numerical model. *Geochemistry, Geophysics, Geosystems*, *16*, 3097–3110. https://doi.org/10.1002/2015GC005916

McEwen, G. F. (1912). The distribution of ocean temperatures along the west coast of North America deduced from Ekman's theory of the upwelling of cold water from the adjacent ocean depths. *Internationale Revue der gesamten Hydrobiologie und Hydrographie*, *5*(2-3), 243–286. https://doi.org/10.1002/iroh.19120050205

McKinney, P., Tokos, K. S., & Matsumoto, K. (2018). Modeling nearshore-offshore exchange in Lake Superior. *PLoS ONE*, *13*(2), e0193183. https://doi.org/10.1371/journal.pone.0193183

Monsen, N. E., Cloern, J. E., Lucas, L. V., & Monismith, S. G. (2002). A comment on the use of flushing time, residence time, and age as transport time scales. *Limnology and Oceanography*, *47*(5), 1545–1553. https://doi.org/10.4319/lo.2002.47.5.1545

Mortimer, C. H. (1952). Water movements in lakes during summer stratification; evidence from the distribution of temperature in Windermere. *Philosophical Transactions of the Royal Society of London. Series B, Biological Sciences*, *236*(635), 355–398. https://doi.org/10.1098/rstb.1952.0005

O'Reilly, C. M., Sharma, S., Gray, D. K., Hampton, S. E., Read, J. S., Rowley, R. J., et al. (2015). Rapid and highly variable warming of lake surface waters around the globe. *Geophysical Research Letters*, *42*, 10,773–10,781. https://doi.org/10.1002/2015GL066235

Peeters, F., Finger, D., Hofer, M., Brennwald, M., Livingstone, D. M., & Kipfer, R. (2003). Deep-water renewal in Lake Issyk-Kul driven by differential cooling. *Limnology and Oceanography*, *48*(4), 1419–1431. https://doi.org/10.4319/lo.2003.48.4.1419

Perroud, M., Goyette, S., Martynov, A., Beniston, M., & Anneville, O. (2009). Simulation of multiannual thermal profiles in deep Lake Geneva: A comparison of one-dimensional lake models. *Limnology and Oceanography*, *54*(5), 1574–1594. https://doi.org/10.4319/lo.2009.54.5.1574

Pöschke, F., Lewandowski, J., Engelhardt, C., Preuß, K., Oczipka, M., Ruhtz, T., & Kirillin, G. (2015). Upwelling of deep water during thermal stratification onset—A major mechanism of vertical transport in small temperate lakes in spring? *Water Resources Research*, *51*, 9612–9627. https://doi.org/10.1002/2015WR017579

Rao, Y. R., Howell, T., Watson, S. B., & Abernethy, S. (2014). On hypoxia and fish kills along the north shore of Lake Erie. *Journal of Great Lakes Research*, *40*(1), 187–191. https://doi.org/10.1016/j.jglr.2013.11.007

Rao, Y. R., & Murthy, C. R. (2001). Nearshore currents and turbulent exchange processes during upwelling and downwelling events in Lake Ontario. *Journal of Geophysical Research*, *106*(C2), 2667–2678. https://doi.org/10.1029/2000JC900149

Rimet, F., Anneville, O., Barbet, D., Chardon, C., Crépin, L., Domaizon, I., et al. (2020). The Observatory on LAkes (OLA) database: Sixty years of environmental data accessible to the public: The Observatory on LAkes (OLA) database. *Journal of Limnology*. Advance online publication, *79*(2). https://doi.org/10.4081/jlimnol.2020.1944

Rivas, D., & Samelson, R. M. (2011). A numerical modeling study of the upwelling source waters along the Oregon Coast during 2005. *Journal of Physical Oceanography*, *41*(1), 88–112. https://doi.org/10.1175/2010JPO4327.1

Sahoo, G. B., Schladow, S. G., Reuter, J. E., Coats, R., Dettinger, M., Riverson, J., et al. (2013). The response of Lake Tahoe to climate change. *Climatic Change*, *116*(1), 71–95. https://doi.org/10.1007/s10584-012-0600-8

Schladow, S. G., Pálmarsson, S. Ó., Steissberg, T. E., Hook, S. J., & Prata, F. E. (2004). An extraordinary upwelling event in a deep thermally stratified lake. *Geophysical Research Letters*, *31*, L15504. https://doi.org/10.1029/2004GL020392

Schulz, B. (1917). Die Auftrieberscheinungen an der Westküste Nordamerikas. *Naturwissenschaften*, *5*(48), 713–719. https://doi.org/10.1007/BF02447973

Selker, J. S., Thévenaz, L., Huwald, H., Mallet, A., Luxemburg, W., van de Giesen, N., et al. (2006). Distributed fiber-optic temperature sensing for hydrologic systems. *Water Resources Research*, *42*, W12202. https://doi.org/10.1029/2006WR005326

Soulignac, F., Danis, P.-A., Bouffard, D., Chanudet, V., Dambrine, E., Guénand, Y., et al. (2018). Using 3D modeling and remote sensing capabilities for a better understanding of spatio-temporal heterogeneities of phytoplankton abundance in large lakes. *Journal of Great Lakes Research*, *44*(4), 756–764. https://doi.org/10.1016/j.jglr.2018.05.008

Steissberg, T. E., Hook, S. J., & Schladow, S. G. (2005). Characterizing partial upwellings and surface circulation at Lake Tahoe, California-Nevada, USA with thermal infrared images. *Remote Sensing of Environment*, *99*(1-2), 2–15. https://doi.org/10.1016/j.rse.2005.06.011

Sun, D., Ito, T., & Bracco, A. (2017). Oceanic uptake of oxygen during deep convection events through diffusive and bubble-mediated gas exchange. *Global Biogeochemical Cycles*, *31*, 1579–1591. https://doi.org/10.1002/2017GB005716

Tamsitt, V., Drake, H. F., Morrison, A. K., Talley, L. D., Dufour, C. O., Gray, A. R., et al. (2017). Spiraling pathways of global deep waters to the surface of the Southern Ocean. *Nature Communications*, *8*(1), 172. https://doi.org/10.1038/s41467-017-00197-0

Thorade, H. (1909). Über die Kalifornischen Meeresströmungen, Oberflächentemperaturen und Strömungen, an der Westküste Nordamerikas. *Annalen der Hydrographie und Maritimen Meteorologie*, *37*(17–34), 63–77.

Thorpe, S. A., Lemmin, U., Perrinjaquet, C., & Fer, I. (1999). Observations of the thermal structure of a lake using a submarine. *Limnology and Oceanography*, *44*(6), 1575–1582. https://doi.org/10.4319/lo.1999.44.6.1575

Troy, C. D., Ahmed, S., Hawley, N., & Goodwell, A. (2012). Cross-shelf thermal variability in southern Lake Michigan during the stratified periods. *Journal of Geophysical Research*, *117*, C02028. https://doi.org/10.1029/2011JC007148

Valipour, R., Rao, Y. R., León, L. F., & Depew, D. (2019). Nearshore-offshore exchanges in multi-basin coastal waters: Observations and three-dimensional modeling in Lake Erie. *Journal of Great Lakes Research*, *45*(1), 50–60. https://doi.org/10.1016/j.jglr.2018.10.005

van de Giesen, N., Steele-Dunne, S. C., Jansen, J., Hoes, O., Hausner, M. B., Tyler, S., & Selker, J. (2012). Double-ended calibration of fiber-optic Raman spectra distributed temperature sensing data. *Sensors*, *12*(5), 5471–5485. https://doi.org/10.3390/s120505471

van Sebille, E., Griffies, S. M., Abernathey, R., Adams, T. P., Berloff, P., Biastoch, A., et al. (2018). Lagrangian ocean analysis: Fundamentals and practices. *Ocean Modelling*, *121*, 49–75. https://doi.org/10.1016/j.ocemod.2017.11.008

Viglione, G. A., & Thompson, A. F. (2016). Lagrangian pathways of upwelling in the Southern Ocean. *Journal of Geophysical Research: Oceans*, *121*, 6295–6309. https://doi.org/10.1002/2016JC011773

Voudouri, A., Avgoustoglou, E., & Kaufmann, P. (2017). Impacts of observational data assimilation on operational forecasts. In T. Karacostas, A. Bais, & P. T. Nastos (Eds.), *Perspectives on Atmospheric Sciences* (pp. 143–149). Cham: Springer International Publishing. https://doi.org/10.1007/978-3-319-35095-0_21

Wahl, B., & Peeters, F. (2014). Effect of climatic changes on stratification and deep-water renewal in Lake Constance assessed by sensitivity studies with a 3D hydrodynamic model. *Limnology and Oceanography*, *59*(3), 1035–1052. https://doi.org/10.4319/lo.2014.59.3.1035

Wang, Y., Hutter, K., & Bäuerle, E. (2000). Wind-induced baroclinic response of Lake Constance. *Annales Geophysicae*, *18*(11), 1488–1501. https://doi.org/10.1007/s005850000279

Woolf, D. K. (1993). Bubbles and the air-sea transfer velocity of gases. *Atmosphere-Ocean*, *31*(4), 517–540. https://doi.org/10.1080/07055900.1993.9649484

References From the Supporting Information

Cole, J. J., & Caraco, N. F. (1998). Atmospheric exchange of carbon dioxide in a low-wind oligotrophic lake measured by the addition of SF 6. *Limnology and Oceanography*, *43*(4), 647–656. https://doi.org/10.4319/lo.1998.43.4.0647

Crusius, J., & Wanninkhof, R. (2003). Gas transfer velocities measured at low wind speed over a lake. *Limnology and Oceanography*, *48*(3), 1010–1017. https://doi.org/10.4319/lo.2003.48.3.1010

Guérin, F., Abril, G., Serça, D., Delon, C., Richard, S., Delmas, R., et al. (2007). Gas transfer velocities of CO_2 and CH_4 in a tropical reservoir and its river downstream. *Journal of Marine Systems*, *66*(1-4), 161–172. https://doi.org/10.1016/j.jmarsys.2006.03.019

Jähne, B., Münnich, K. O., Bösinger, R., Dutzi, A., Huber, W., & Libner, P. (1987). On the parameters influencing air-water gas exchange. *Journal of Geophysical Research*, *92*(C2), 1937–1949. https://doi.org/10.1029/JC092iC02p01937

Klaus, M., & Vachon, D. (2020). Challenges of predicting gas transfer velocity from wind measurements over global lakes. *Aquatic Sciences*, *82*(3), 53. https://doi.org/10.1007/s00027-020-00729-9

Mortimer, C. H. (1981). The oxygen content of air-saturated fresh waters over ranges of temperature and atmospheric pressure of limnological interest. *SIL Communications, 1953-1996*, *22*(1), 1–23. https://doi.org/10.1080/05384680.1981.11904000

Vachon, D., & Prairie, Y. T. (2013). The ecosystem size and shape dependence of gas transfer velocity versus wind speed relationships in lakes. *Canadian Journal of Fisheries and Aquatic Sciences*, *70*(12), 1757–1764. https://doi.org/10.1139/cjfas-2013-0241

Wanninkhof, R. (2014). Relationship between wind speed and gas exchange over the ocean revisited: Gas exchange and wind speed over the ocean. *Limnology and Oceanography: Methods*, *12*, 351–362. https://doi.org/10.4319/lom.2014.12.351